

Investigation on the Volatility of Ammonium Nitrate Using Optical Tweezers

LÜ Xi-juan, GAO Xiao-yan, MA Jia-bi*, ZHANG Yun-hong*

Institute of Chemical Physics, School of Chemistry and Chemical Engineering, Beijing Institute of Technology, Beijing 100081, China

Abstract Measurements of the particle-to-gas partitioning of semi-volatile atmospheric aerosols are crucial for providing more accurate descriptions of the compositional and size distributions of atmospheric aerosol. As a major component of semi-volatile aerosol species, ammonium nitrate (NH_4NO_3) is ubiquitous in the sub-micron particulate matter, particularly in high pollution episodes. In order to further understand gas-particle partitioning of NH_4NO_3 , determination of the saturated vapor pressure of NH_4NO_3 is needed. Here, we investigate the volatility of NH_4NO_3 at different relative humidities (RHs) using aerosol optical tweezers coupled with Raman spectroscopy as an instrument for sampling and detecting. According to the Maxwell equation, the vapor pressures at different RHs are calculated, and the values are $(1.67 \pm 0.24) \times 10^{-3}$, $(1.82 \pm 0.19) \times 10^{-3}$, $(2.91 \pm 0.13) \times 10^{-3}$, $(3.5 \pm 0.28) \times 10^{-3}$, $(4.59 \pm 0.22) \times 10^{-3}$ and $(6.64 \pm 0.3) \times 10^{-3}$ Pa, when the RH is 80%, 73%, 68%, 57.3%, 55.4%, 44.8% respectively. Obviously, the vapor pressures of NH_4NO_3 increase with RH decreasing, i. e. low RH promotes the evaporation of ammonium nitrate. Additionally, we also calculate the volatilizing flux of NH_4NO_3 at different RHs, and the values are in the range of $(4.01 \pm 0.79) \times 10^{-7} \sim (3.32 \pm 0.77) \times 10^{-8}$ mol \cdot (s \cdot m²)⁻¹. The results obtained herein are of important significance in understanding the partitioning processes of semi-volatile aerosols.

Keywords Aerosol; Optical tweezers; Ammonium nitrate; Volatility; Vapor pressures

中图分类号: O657.3 文献标识码: A DOI: 10.3964/j.issn.1000-0593(2019)05-1648-05

Introduction

Aerosol particles are important constituents of the atmosphere. They impact modern society through their effects on visibility, human health, and global climate. In atmospheric and climate science there is considerable interest in understanding the partitioning between gas and particle phase of chemical species. In particular, for semi-volatile substances like NH_4NO_3 , the partitioning will strongly influence the particulate matter burden in the troposphere, the radiative properties of the aerosol, the cloud processing and the heterogeneous chemistry.

NH_3 is the dominant volatile base in the atmosphere,

with their main sources stemming from combustion, fertilizers and biological decay^[1]. By reacting with H_2SO_4 , HNO_3 and HCl , ammonium salts such as $(\text{NH}_4)_2\text{SO}_4$, NH_4NO_3 and NH_4Cl are formed and account for the predominant inorganic components of atmospheric aerosols^[2]. Unlike most of the other hygroscopic salts found in the atmosphere, NH_4NO_3 is a salt with a relatively high vapor pressure. Particles containing NH_4NO_3 are in equilibrium with gaseous NH_3 and HNO_3 and the partitioning between particle and gas is a strong function of temperature and relative humidity^[3]. In order to predict this partitioning, it is crucial to know the vapor pressure of the NH_4NO_3 under ambient conditions.

Many techniques have been developed to measure the evaporation of monodisperse NH_4NO_3 under different RHs by

Received: 2018-03-30; accepted: 2018-08-05

Foundation item: National Key R&D Program of China (2016YFC0203000), Natural Science Foundation of China (91644101, 91544223)

Biography: LÜ Xi-juan, (1986—), Post-doctoral of Beijing Institute of Technology e-mail: 7520180040@bit.edu.cn

* Corresponding authors e-mail: majiabi@bit.edu.cn; yhz@bit.edu.cn

continuously and rapidly removing gaseous NH_3 and HNO_3 from aerosols. Hu, et al.^[4] investigated the effects of RH and particle size on evaporation of NH_4NO_3 aerosols by a self-assembled hygroscopic tandem differential mobility analyzer (H-TDMA) system. They found that the evaporation of NH_4NO_3 particle less than 50 nm was significantly promoted while RH increased below the DRH. The proposed mechanism suggested that the increase of RH alters the chemical equilibrium, i. e., $\text{NH}_4\text{NH}_3(\text{s}) \rightleftharpoons \text{NH}_3(\text{g}) + \text{HNO}_3(\text{g})$, by converting $\text{NH}_3(\text{g})$ and $\text{HNO}_3(\text{g})$ into $\text{NH}_3 \cdot n\text{H}_2\text{O}$ and $\text{HNO}_3 \cdot n\text{H}_2\text{O}$, which accelerated the evaporation of $\text{NH}_4\text{NO}_3(\text{s})$. Chien, et al.^[5] determined the total vapor pressure of NH_4NO_3 over the range of 313~360 K, and the values were $8.073 \times 10^{-3} \sim 1.057$ Pa. The vapor pressure was determined by the torsion and effusion method, and vapor composition was determined by effusion-beam mass spectrometry. Hong, et al.^[6] obtained the effective saturation vapor concentration for NH_4NO_3 field measurements using a volatility tandem differential mobility analyzer (VTDMA) with a kinetic evaporation model. According to the saturation vapor concentration obtained for NH_4NO_3 , they concluded that NH_4NO_3 can be considered as semi-volatile compounds and the value of vapor pressure was 2.6×10^{-3} Pa. Zardini, et al.^[7] described how a time series of optical resonance spectra of an evaporating, non-spherical, irregular aerosol particle levitated in an electrodynamic balance exhibited patterns which were related to its evaporation kinetics, and the vapor pressures of solid NH_4NO_3 from evaporating particles over the range of 278.2~303.15 K were $(5.52 \pm 1.93) \times 10^{-5} \sim (2.03 \pm 0.71) \times 10^{-3}$ Pa. However, the saturated vapor pressure of NH_4NO_3 at different RH at room temperature has not been found.

In this paper, we use a new technique for exploring the equilibrium properties of ammonium nitrate aqueous aerosol particles using optical tweezers coupled with cavity-enhanced Raman spectroscopic. The particle is confined in three dimensions, and can be held indefinitely by the optical forces. Rather than attempting to isolate the gas-particle partitioning of water and the semi-volatile compounds in independent measurements, the technique is instead derived from exploiting the intimate coupling between the two^[8]. Simultaneous and accurate measurements of the refractive index and size of aqueous aerosol can allow parallel estimations of the change in composition as well as size, providing concurrent information on the gas-particle partitioning of both the semi-volatile compounds and water. In this work, the vapor pressures of NH_4NO_3 aerosols (2~10 μm) are measured from 44.8% to 80% RH using an optical tweezers coupled with cavity-enhanced Raman spectroscopic. The effects of RH on the evaporation of NH_4NO_3 aerosols are discussed.

1 Experimental description

The aerosol optical tweezers setup has been comprehensively described in previous publications and we only briefly summarize the key elements^[9-10]. Fig. 1 shows a schematic diagram of the single gradient force optical trap used in this study. The optical trap is formed by focusing the beam (532 nm, 200 mW) from an argon-ion laser (Opus 4 W+mpc6000 power supply) through an Olympus UIS2 PlanCN 100 \times oil immersion objective (1.25 N. A.). A blue LED centered at 455 nm is adopted as the illumination source for bright-field imaging of the trapped droplets received by a camera (Watec, 1/3 in., model 231S2). Droplets of 1 mol \cdot L⁻¹ NH_4NO_3 solution are introduced into the sample cell and a single droplet from the cloud is captured. The RH of the gas phase is controlled from dry conditions (<5% RH) to high RH (>80%) by mixing flows of dry and humidified nitrogen. The flow rates are controlled by two independent mass flow controllers (Alicat Scientific No. 21-1-08-1-1-KM0410). The combined gas flow introduced into the cell is kept constant at 0.20 L \cdot min⁻¹. The RH and the temperature of the combined gas flow are measured by RH-T detectors (Center 313) before the cell and in the outflow from the cell. The uncertainty of RH determination is $\pm 2.5\%$. Particles are imaged by brightfield microscopy. Inelastic backscattered light collected by the microscope objective is imaged into a 0.5 m focal length spectrograph, dispersed by a 1200 $\text{g} \cdot \text{mm}^{-1}$ grating, and the Raman spectrum recorded by a CCD with a time resolution of 1 s and a spectral dispersion of 0.04 nm per pixel. In addition to the familiar spontaneous Stokes bands shifted from the excitation wavelength, the Raman spectrum provides a unique fingerprint of droplet size and refractive index (RI) through the

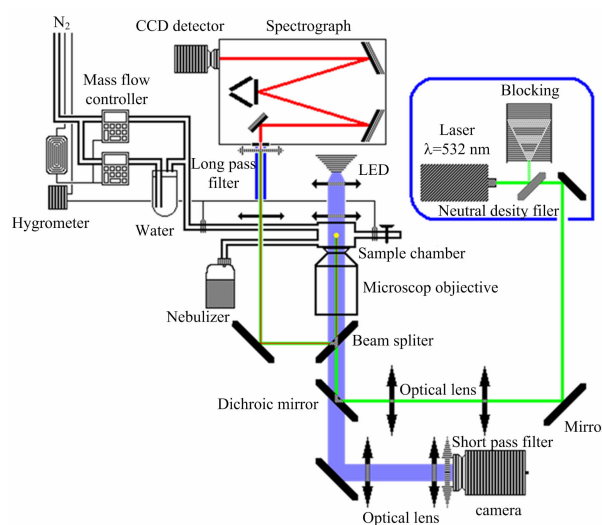


Fig. 1 Schematic diagram of experimental set-up used for single droplet optical tweezers

pattern of resonant modes superimposed on the spontaneous band at wavelengths commensurate with whispering gallery modes. The size, RI and dispersion in RI can be retrieved with high accuracy from this fingerprint by comparison with Mie scattering calculations^[11-12].

2 Evaporation kinetics of water and ammonium nitrate

To explore the evaporation kinetics of water and NH_4NO_3 , the aqueous droplets of $\text{NH}_4\text{NO}_3/\text{H}_2\text{O}$ at different constant RHs are optically trapped by optical tweezers. A typical cavity-enhanced Raman spectra (CERS) example of an aqueous $\text{NH}_4\text{NO}_3/\text{H}_2\text{O}$ droplet at 67% RH is shown in Fig. 2 (a). The time evolution of the wavelengths of the WGM resonant modes on the OH band for the $\text{NH}_4\text{NO}_3/\text{H}_2\text{O}$ droplet at 67% RH is shown in Fig. 2(b). During this process, we can find that the Raman peaks are shifted to the lower wavelength during acquisition time when the RH is constant at 67%, and such phenomenon is mainly due to the evaporation of ammonium nitrate. Changes in droplet size and refractive index are shown in Fig. 3. The decrease of the radius reflects the volatility of the droplet.

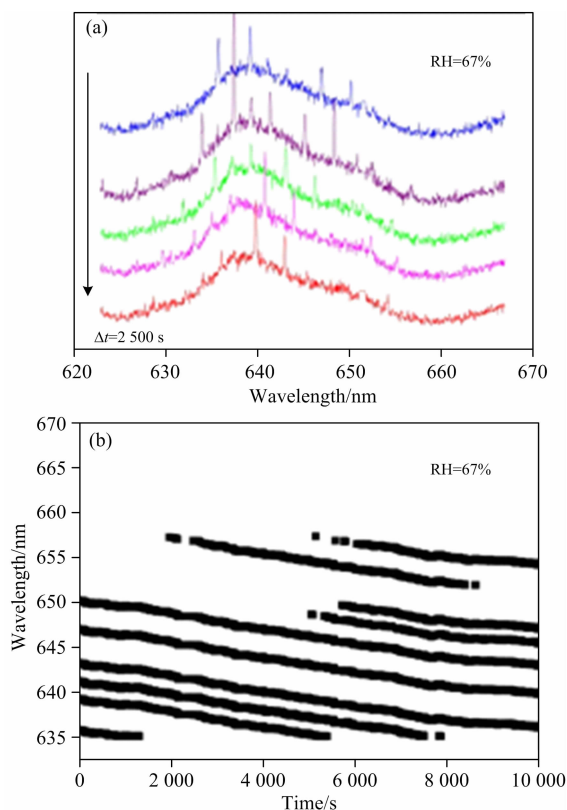


Fig. 2 (a) CERS of $\text{NH}_4\text{NO}_3/\text{H}_2\text{O}$ droplet at 67% RH; (b) The time evolution of the wavelengths of the WGM resonant modes on the OH band for the $\text{NH}_4\text{NO}_3/\text{H}_2\text{O}$ droplet at 67% RH

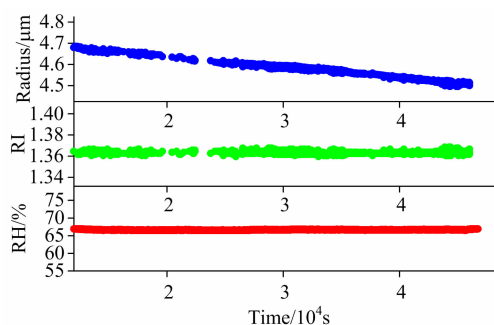


Fig. 3 Time-dependent $\text{NH}_4\text{NH}_3/\text{H}_2\text{O}$ droplet size (blue line), RI (green line) and RH (red line) at 298 K in the laser tweezers apparatus are presented

The evaporation experiments are repeated at other constant RHs and the same analysis as described above is performed. The effective pure component vapor pressure of ammonium nitrate can be estimated from the rate of change in the radius-squared of an aqueous droplet (r^2) held at a constant RH with time (t) due to the evaporation of ammonium nitrate. Since an evaporating of ammonium nitrate particle dissociates in ammonia and nitric acid through the reaction: $\text{NH}_4\text{NH}_3(\text{l}) \rightleftharpoons \text{NH}_3(\text{g}) + \text{HNO}_3(\text{g})$, the vapor pressure can be determined from radius change via the Maxwell equation^[7, 13]

$$p = p_{\text{NH}_3} + p_{\text{HNO}_3} = -\frac{1}{2} \frac{dr^2}{dt} RT \frac{\rho_{\text{AN}} F_i}{M_{\text{AN}} \chi_i f_i} \left(\frac{1}{D_{\text{NH}_3}} + \frac{1}{D_{\text{HNO}_3}} \right) \quad (1)$$

where M_{AN} is the molecular mass of ammonium nitrate, D_{NH_3} and D_{HNO_3} are the diffusivities of the two species in the ambient air, R is the ideal gas constant, T is the temperature, f_i is the activity coefficient, ρ_{AN} is the density of the droplet and F_i is the mass fraction of ammonium nitrate in the droplet. Diffusivities for HNO_3 and NH_3 are taken from Xue et al.^[14] and Massman^[15].

The effective pure component vapor pressures of NH_4NO_3 at different constant RHs are calculated according to equation (1), and the results are presented in Fig. 4. The effective pure component vapour pressures of ammonium nitrate are $(1.67 \pm 0.24) \times 10^{-3}$, $(1.82 \pm 0.19) \times 10^{-3}$, $(2.91 \pm 0.13) \times 10^{-3}$, $(3.5 \pm 0.28) \times 10^{-3}$, $(4.59 \pm 0.22) \times 10^{-3}$ and $(6.64 \pm 0.3) \times 10^{-3}$ Pa, when the RH is 80%, 73%, 68%, 57.3%, 55.4%, 44.8% respectively. The vapour pressure of ammonium nitrate is of the same magnitude as in previous studies^[5-6, 16]. In the range of RH studied here, the saturated vapor pressure of ammonium nitrate increases with the decrease of RH. This shows that the lower the RH is, the easier the ammonium nitrate evaporates.

The volatilizing flux of NH_4NO_3 can be estimated from the rate of change in the volume of droplets and the concentration of NH_4NO_3 (inferred from refractive index). The calcula-

tion formula is as follows:

$$F = \frac{4}{3}\pi(r_0^3 - r^3)c_0/4\pi r^2 t \quad (2)$$

where r_0 is initial radius, c_0 is the concentration of NH_4NO_3 , r is the real-time radius.

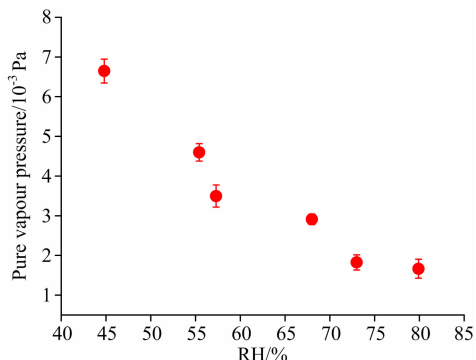


Fig. 4 Pure vapor pressures of NH_4NO_3 at different constant RHs

Volatilizing flux of the ammonium nitrate at each constant RH (estimated from equation (2)) are shown in Fig. 5. The volatile flux of ammonium nitrate is in the range of $(4.01 \pm 0.79) \times 10^{-7} \sim (3.32 \pm 0.77) \times 10^{-8} \text{ mol} \cdot (\text{s} \cdot \text{m}^2)^{-1}$.

3 Conclusions

We report the equilibrium properties of NH_4NO_3 aqueous aerosol particles using optical tweezers coupled with cavity-enhanced Raman spectroscopic. The vapor pressures at

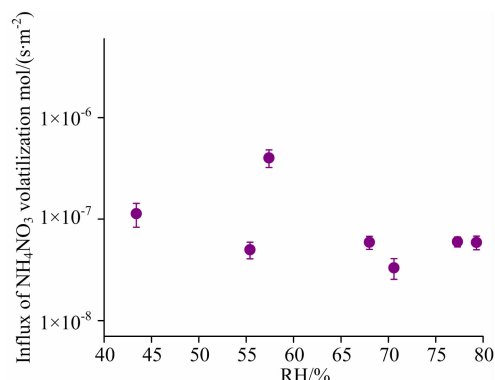


Fig. 5 Volatilizing fluxes of NH_4NO_3 at different constant RHs

different constant RHs are calculated according to the Maxwell equation and the values are $(1.67 \pm 0.24) \times 10^{-3}$, $(1.82 \pm 0.19) \times 10^{-3}$, $(2.91 \pm 0.13) \times 10^{-3}$, $(3.50 \pm 0.28) \times 10^{-3}$, $(4.59 \pm 0.22) \times 10^{-3}$ and $(6.64 \pm 0.3) \times 10^{-3}$ Pa when the RH is 80%, 73%, 68%, 57.3%, 55.4%, 44.8% respectively. These values are of the same magnitude as that in previous studies. With decreasing RH, the vapor pressure of NH_4NO_3 increases, indicating that the low RH accelerates the evaporation of NH_4NO_3 . In addition, the volatile fluxes of ammonium nitrate are also calculated at different RHs and they are in the range of $(4.01 \pm 0.79) \times 10^{-7} \sim (3.32 \pm 0.77) \times 10^{-8} \text{ mol} \cdot (\text{s} \cdot \text{m}^2)^{-1}$.

Acknowledgment

The authors wish to express their gratitude to the anonymous reviewers for the stimulating suggestions and discussions.

References

- [1] Bouwman A F, Lee D S, Asman W A H, et al. *Global Biogeochemical Cycles*, 1997, 11(4): 561.
- [2] Renard J J, Calidonna S E, Henley M V. *Journal of Hazardous Materials B*, 2004, 108(1-2): 29.
- [3] James M, Lightstone T B O, Dan Imre. *Journal of Physical Chemistry A*, 2000, 104(41): 9337.
- [4] Hu Dawei, Chen Jianmin, Ye Xingnan, et al. *Atmospheric Environment*, 2011, 45(14): 2349.
- [5] Chien Wen-ming, Chandra Dhanesh, Lau K H, et al. *The Journal of Chemical Thermodynamics*, 2010, 42(7): 846.
- [6] Hong J, Äijälä Mikko, Häme S A K, et al. *Atmospheric Chemistry and Physics*, 2017, 17(6): 4387.
- [7] Zardini A A, Krieger U K. *Optics Express*, 2009, 17(6): 4659.
- [8] Cai C, Stewart D J, Reid J P, et al. *Journal of Physical Chemistry A*, 2015, 119(4): 704.
- [9] Wang L N, Cai C, Zhang Y H. *Journal of Physical Chemistry B*, 2017, 121(36): 8551.
- [10] Cai C, Tan S, Chen H, et al. *Physical Chemistry Chemical Physics*, 2015, 17(44): 29753.
- [11] Preston T C, Reid J P. *Journal of the Optical Society of America B*, 2013, 30(8): 2113.
- [12] Miles R E, Walker J S, Burnham D R, et al. *Physical Chemistry Chemical Physics*, 2012, 14(9): 3037.
- [13] Marshall F H, Miles R E H, Song Y C, et al. *Chemical Science*, 2016, 7(2): 1298.
- [14] Xue H, Moyle A M, Magee N, et al. *Journal of the Atmospheric Sciences*, 2005, 62(12): 4310.
- [15] Massman W J. *Atmospheric Environment*, 1998, 32(6): 1111.
- [16] Huffman J A, Docherty K S, Aiken A C, et al. *Atmospheric Chemistry and Physics Discussions*, 2009, 9(1): 2645.

用光镊技术研究硝酸铵气溶胶的挥发性

吕席卷, 高晓艳, 马嘉璧*, 张韫宏*

北京理工大学化学与化工学院, 化学物理研究所, 北京 100081

摘要 研究半挥发性气溶胶物质的气粒分配对于更准确地描述大气气溶胶的组成和尺寸分布是至关重要的。硝酸铵是亚微米颗粒物的主要组成部分, 特别是在高污染事件中。为了更深入的了解硝酸铵气溶胶的气粒分配问题, 利用激光悬浮技术捕获、悬浮半挥发性无机物硝酸铵液滴单颗粒($2\sim 10\ \mu\text{m}$), 控制相对湿度条件、温度条件, 并采集氢-氧振动带的受激拉曼峰位信息, 利用非弹性米氏散射理论计算实时液滴半径尺寸、折射率和浓度, 利用稳态传质模型 Maxwell 公式推算出了不同湿度下的蒸汽压。实验数据计算出的硝酸铵的饱和蒸汽压值的数量级与文献报道一致。当 RH 分别恒定在 80%, 73%, 68%, 57.3%, 55.4%, 44.8% 时, 饱和蒸汽压值为 $(1.67\pm 0.24)\times 10^{-3}$, $(1.82\pm 0.19)\times 10^{-3}$, $(2.91\pm 0.13)\times 10^{-3}$, $(3.5\pm 0.28)\times 10^{-3}$, $(4.59\pm 0.22)\times 10^{-3}$ 和 $(6.64\pm 0.3)\times 10^{-3}$ Pa, 显然, 随着相对湿度的降低, 饱和蒸汽压值增大, 即湿度降低促进硝酸铵的挥发。此外, 还推算了不同湿度下硝酸铵气溶胶液滴的挥发通量, 挥发通量值在 $(4.01\pm 0.79)\times 10^{-7}\sim (3.32\pm 0.77)\times 10^{-8}$ $\text{mol}\cdot(\text{s}\cdot\text{m}^2)^{-1}$ 之间。这对更好的了解气溶胶在挥发过程中的微观过程有重要意义。

关键词 气溶胶; 光镊技术; 硝酸铵; 挥发性; 蒸发压力

(收稿日期: 2018-03-30, 修订日期: 2018-08-05)

* 通讯联系人